JOURNAL OF SPACECRAFT AND ROCKETS
Vol. 35, No. 1, January–February 1998

Orbit Plane Control Strategies for Inclined Geosynchronous Satellite Constellation

Jean Albert Kechichian*
The Aerospace Corporation, El Segundo, California 90245

The dynamics and control of the motion of the orbit planes of a constellation of five satellites in inclined geosynchronous orbits are analyzed. Orbit maintenance strategies that confine each individual orbit inclination within a predefined tolerance deadband are designed using fast analytic orbit prediction approximations, as well as more exacting numerically integrated solutions. The initial orbit inclination of each satellite is chosen optimally within the tolerance band such that each satellite orbit remains confined within the limits of the band for the longest possible time before an inclination adjust maneuver is carried out. The total ΔV required by each satellite over the constellation lifetime is, thus, rapidly determined, and the ideal initial nodes of the initially evenly spaced orbit planes that result in the minimum total ΔV accumulated by all five satellites are established. This total ΔV is also shown to be dependent on the ecliptic node of the lunar orbit within its 18.6-year regression cycle. A more elaborate scheme that maintains the orbit planes evenly spaced at the equator by controlling each satellite node is also depicted analytically, to optimize the initial nodal configuration that minimizes the total accumulated ΔV of all five satellites over the constellation lifetime.

Nomenclature

i_M = ecliptic inclination of the lunar orbit
i_m = equatorial inclination of the lunar orbit
$i_{\max}$ = maximum orbit inclination
$i_{\min}$ = minimum orbit inclination
i_s = sun's apparent orbit equatorial inclination
i^* = wedge angle between premaneuver and postmaneuver orbits
J_2 = Earth second zonal harmonic, 1.0827×10^{-3}
n = satellite orbit mean motion
n_m = lunar orbit mean motion, 0.23 rad/day
n_s = apparent solar orbit mean motion, 0.017203 rad/day
R = perturbing function due to J_2 and lunisolar gravity
R_e = Earth equatorial radius, 6378.14 km
μ = ratio of the mass of the moon to the combined masses of the Earth and the moon, 1/82.3
μ_e = Earth gravity constant, 398,601.3 km^3/s^2
Ω_M = ecliptic ascending node of the lunar orbit
Ω_m = right ascension of the ascending node of the lunar orbit

Introduction

THE inclination i and the ascending node Ω of a satellite in geosynchronous condition are affected by the perturbations due to the triaxiality of the Earth, as well as the gravitational perturbations due to the sun and the moon.[1–13] Single-satellite control strategies are depicted in Refs. 6, 8, 11, 12, and 14. References 15, 16, and in particular 17 address the dynamics and control of a cluster of satellites in geostationary orbit with the cluster residing within well-defined limits in longitude and latitude. The present paper considers the problem of the orbit plane control of a constellation of geosynchronous satellites whose orbits are identically inclined and with evenly spaced ascending nodes. It is assumed that each orbit plane contains a single satellite. Given a constellation lifetime, it is desired to maintain each satellite orbit inclination within a small tolerance band centered at their nominal inclination and to determine the total accumulated ΔV required by each satellite during its lifetime. The control strategies developed for the geostationary satellites are no longer applicable here because the nominal inclination is not near zero but at 12 deg for our application at hand. Furthermore, the ideal even spacing in nodes at the initial time is distorted if left uncontrolled because each satellite orbit starts from a different node and, therefore, experiences a different nodal rate that in time upsets the evenly spaced nodal distribution. Using a combination of graphical, analytical, and numerical techniques, the following sections show orbit maintenance strategies that control either the inclination or both the inclination and the node of each satellite such that the tolerance band in inclination is never violated and, in the latter case, the evenly spaced nodal configuration is maintained over the constellation lifetime. Thus, the ΔV requirements for each satellite are rapidly determined. These requirements, being dependent on both the initial nodal configuration of the evenly spaced constellation and the lunar orbit ecliptic node, are in turn minimized by the optimal selection of the initial nodes for a given start time and by the optimal selection of both the initial nodes and the start time within the 18.6-year regression cycle of the lunar orbit ecliptic node.

Presented as Paper 95-342 at the AAS/AIAA Astrodynamics Conference, Halifax, NS, Canada, Aug. 14–17, 1995; received March 18, 1997; revision received July 29, 1997; accepted for publication Aug. 10, 1997.

*Engineering Specialist, Astrodynamics Department, 2350 E. El Segundo Boulevard. Associate Fellow AIAA.

General Discussion

For 24-h, near-equatorial circular orbits, an inclination deadband is defined and the satellite is placed initially at the maximum allowed inclination with an appropriate node Ω such that a maximum period of free drift takes place with both i and Ω varying and such that i is decreasing during the first half of that period and increasing for the other half until the inclination constraint is violated.[9,18] An impulsive maneuver is then applied to target certain ideal initial conditions in i and Ω such that the subsequent motion of the orbit plane complies with the inclination tolerance until the end of the mission. For small deadbands, these ideal initial conditions can be selected in such a manner that the time between two successive maneuvers is maximized. However, this simple orbit maintenance scheme becomes much more complicated if the satellite orbit is inclined at a much larger angle with respect to the equator. Unlike the near-equatorial case where the inclination deadband is defined by $0 \leq i \leq i_{\max}$, the deadband is now defined by $i_{\min} \leq i \leq i_{\max}$. The maximum duration free drift mentioned is no longer feasible because i will violate the $i_{\min}$ constraint before the completion of the drift. Furthermore, the satellites being placed in five different planes evenly spaced in Ω, their Ω-drift rates are not identical, resulting in the distortion of the nodal spacing with time.

In a first analysis, use is made of the fact that the orbit planes of the five satellites oscillate slowly about the dynamically steady invariant plane inclined roughly at 7.5 deg. Furthermore, adopting the h_1, h_2 plane to depict the various orbit plane precessions, with $h_1 = s_i s_\Omega$ and $h_2 = s_i c_\Omega$ and with s_i and c_i standing for sin

and cos i, respectively, an inclination deadband in the form of an annulus is defined, consisting of the region confined between the two concentric circles centered at $h_1 = h_2 = 0$ with respective radii of $s_{i_{\min}}$ and $s_{i_{\max}}$. The nonsingular variables h_1 and h_2 effectively replace the pair i, Ω because the coupled system of differential equations for i and Ω has a singularity at $i = 0$. Thus, the adoption of h_1 and h_2 extends the applicability of this analysis to the near-equatorial case without any restrictions. A target locus confined to the tolerance annulus is also defined, consisting of four separate curves depending on the range of Ω, such that the impulsive maneuvers always target the orbit plane orientation parameters to given points on this locus curve. The symmetrical Ω spacing is controlled by adjusting the nodal spacing at the time of the inclination control maneuvers.

This paper shows how these maneuvers are mechanized and designed to control the constellation drift within well-defined bounds. Numerical integration is also used to generate more accurate ΔV requirements for the entire constellation. Let us first use approximate graphical techniques consisting of the depiction of the evolution of the projection of the orbital angular momentum vector onto the equatorial plane to obtain preliminary evaluations of the free drift characteristics of the constellation. The precession of a geosynchronous satellite orbit plane about the equilibrium plane at $i = 7.5$ deg and $\Omega = 0$ deg takes roughly 54 years for a complete 360-deg variation in Ω. The inclination deadband for a nominal 12-deg inclination with ± 1 deg tolerance consists of the annulus between the two concentric circles centered at $h_1 = h_2 = 0$ with respective radii of $s_{i_{\min}}$ and $s_{i_{\max}}$ and labeled 11 and 13 deg, respectively, as shown in Fig. 1. The invariant plane is depicted by the point P ($h_1 = 0, h_2 = s_{7.5\,\mathrm{deg}}$) on the h_2 axis and the orbit plane precessions shown by concentric circles centered at P. Each point (h_1, h_2) corresponds to a well-defined orbit plane orientation whose parameters are given by i and Ω. Because of the definitions of h_1 and h_2, a point in the (h_1, h_2) plane has polar coordinates (s_i, Ω) with the angle Ω measured from the h_2 axis and with s_i its distance from the origin 0. Starting from a given i, Ω pair, or equivalently h_1, h_2 pair, the orbit plane will precess such that the subsequent motion in the h_1, h_2 plane describes to the zeroth order a circle centered at the equilibrium point P. Two such precession circles are shown in Fig. 1. Only those portions of these precession circles that are within the annulus are acceptable in the sense that they comply with and satisfy the inclination tolerance deadband.

For small tolerances on the nominal inclination, e.g., of the order of ± 1 or 2 deg, let us adopt the dotted-line EFAGHE as the locus of the initial orbits to target to, such that starting from any point on this locus, it will take the longest possible time for the orbit to violate the inclination deadband constraint. The portions EF and GH are circular arcs centered at P and lying entirely within the annulus. The circular arcs FG and HE are centered at O and lying on the $s_{i_{\max}}$ and $s_{i_{\min}}$ circles, respectively. The tolerance annulus, therefore, can be divided into four parts, namely I, II, III, and IV, as indicated in Fig. 1. The precession rate around P being constant and considering a nominal 10-year constellation lifetime, a nominal 10-year precession will result in an angular motion of nearly 66 deg.

As is shown in Fig. 2, with $i_{\min} = 11$ deg and $i_{\max} = 13$ deg, if we place the common orbit of the five satellites at point E, the precession circle EFI stays for the longest possible time within the tolerance annulus and covers a central angle of 130 deg in roughly 20 years. If we place the orbit plane at G, the precession GHQ will cover only 68 deg before deadband violation. This strategy is also acceptable because it results in a 10-year precession without any maneuvering. Point E corresponds to an initial $\Omega_i = 27$ deg at $i = 11$ deg. Figure 2 also shows a larger deadband with $i_{\min} = 7$ deg and $i_{\max} = 17$ deg or a ± 5-deg tolerance from the nominal $i = 12$ deg inclination. The arc E′F′I′ covers a central angle of 263 deg in nearly 39 years, whereas the arc G′H′Q′ covers an angle of 189 deg in 28 years with

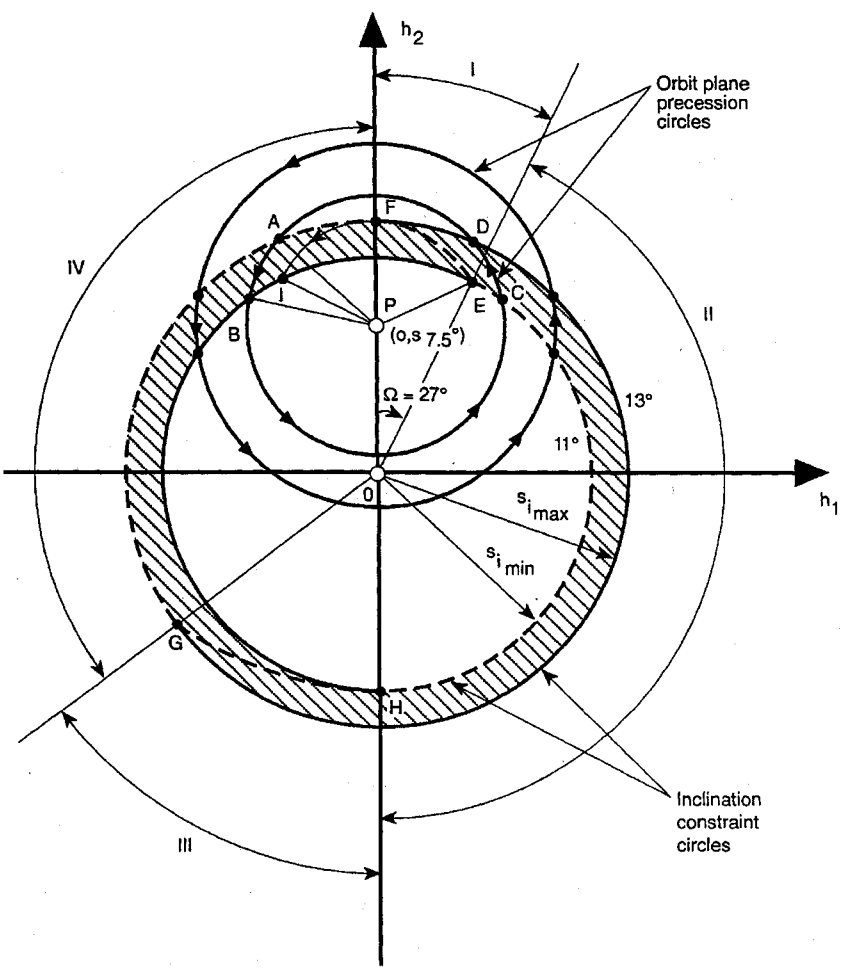

Fig. 1 Inclination deadband for minimum and maximum constraints.

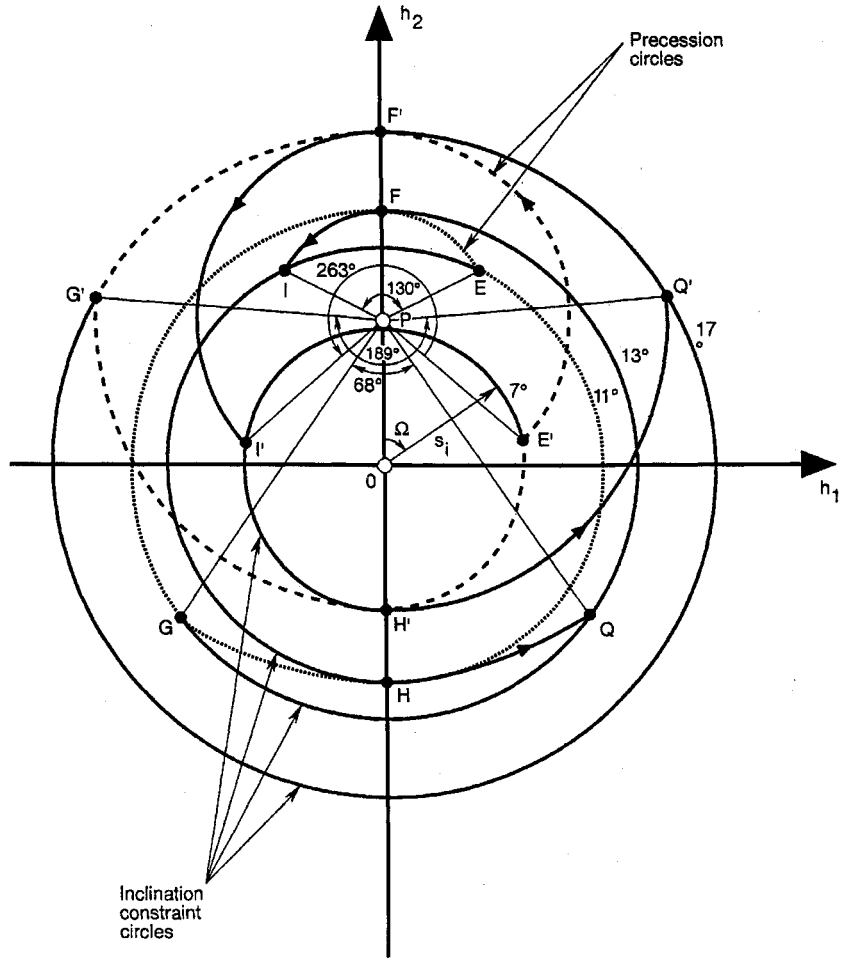

Fig. 2 Maximum duration compliance strategies for given tolerance deadbands with satellites in common orbit plane.

no deadband violation or any maneuvering requirements. There are many more feasible initial orbits that satisfy the 10-year lifetime requirement with no maneuvering for this larger deadband example, as expected.

Let us now consider each satellite flying in a different orbit plane with the five planes equally spaced in Ω. In Fig. 3, i = 12 deg, the nominal value, and the satellite planes are given by Ω = 0, 72, 144, 216, and 288 deg corresponding to the points J, K, L, M, and N with equal spacing of $\Delta\Omega$ = 72 deg. The lines labeled 1–5 identify the five nodal directions. A 10-year precession of the five satellite orbits will result in the precession arcs JJ′, KK′, LL′, MM′, and NN′ each covering an equal central angle of 66 deg at P, the equilibrium point. The smallest and largest inclinations achieved are i = 4.5 and 19.8 deg by satellites 5 and 3 and are measured by the segments ON′ and OL′ equal to the sine of the corresponding inclination. However, the nodes of the orbits are now given by the directions of the lines 1′, 2′, 3′, 4′, and 5′ measured at O from the h_2 axis, showing significant distortion with respect to the initial symmetric configuration. The largest nodal separation is between satellites 1 and 5 with $\Delta\Omega$ = 142 deg or double the initial separation. This indicates that a tolerance deadband in the node must also be considered to maintain proper spacing, besides the inclination deadband discussed so far. There exists an optimum initial Ω configuration that will result in the smallest inclination excursion from the 12-deg nominal inclination at the end of the 10-year drift period. However, the distortion in the initial uniform Ω distribution must also be factored in, and the overall optimum initial configuration must be found to minimize the inclination excursion as well as the Ω distortion. If we move the initial configuration to Ω = 72, 144, 216, 288, and 360 deg, then we will recover the initial configuration of Fig. 3. This means that the smallest inclination excursion in the 10-year drift period corresponding to the optimum initial configuration can be iterated from such figures.

In fact, the locus of all possible precession endpoints at the 10-year mark that originate from the common initial nominal inclination at 12 deg and any initial Ω between 0 and 360 deg is shown in Fig. 4. The smallest and largest final inclinations are shown by the points N′ and M′, with ON′ = $s_{i_{\min}}$ and OM′ = $s_{i_{\max}}$ and with roughly $i_{\min} \approx 3.6$ deg and $i_{\max} \approx 20.1$ deg indicating that the largest change in the inclination is of the order of 8.5 deg. Similar loci can be plotted for different values of the satellite's lifetime to determine the largest possible changes in the inclination over that particular lifetime. The two points of intersection between a given locus and the nominal inclination constraint circle are points that result in zero change in the inclination. For example, the precessions JJ′ and KK′ start and end at the nominal inclination with small and acceptable deviations during the precessions.

Figure 5 shows the h_1, h_2 mappings for the 10-, 20-, 30-, 40-, and 50-year precession endpoints for the 12-deg nominal inclination case. These loci are circles that are rotated about the equilibrium point situated on the h_2 axis by the corresponding precession angles. The 54-year precession case maps the original nominal constraint circle back into itself after a complete 360-deg rotation about the same equilibrium point. This is, in fact, how the satellite orbit plane oscillates slowly about its idealized equilibrium orientation with the period of 54 years.

The mechanization of these approximate zeroth-order analytic precessions is described in Ref. 18 and also briefly in the next section. Initially, the satellite orbits are evenly spaced in Ω and lying on the dotted line of Fig. 1. When one of the satellites reaches the boundary of the annulus, a maneuver must place it back on the dotted curve for another period of free drift. This maneuver can consist of a pure inclination change at constant Ω. However, the other four satellites experience different Ω rates such that they too must be maneuvered back to the dotted curve, but this time, each satellite must also adjust its Ω in such a way that all five orbits are back

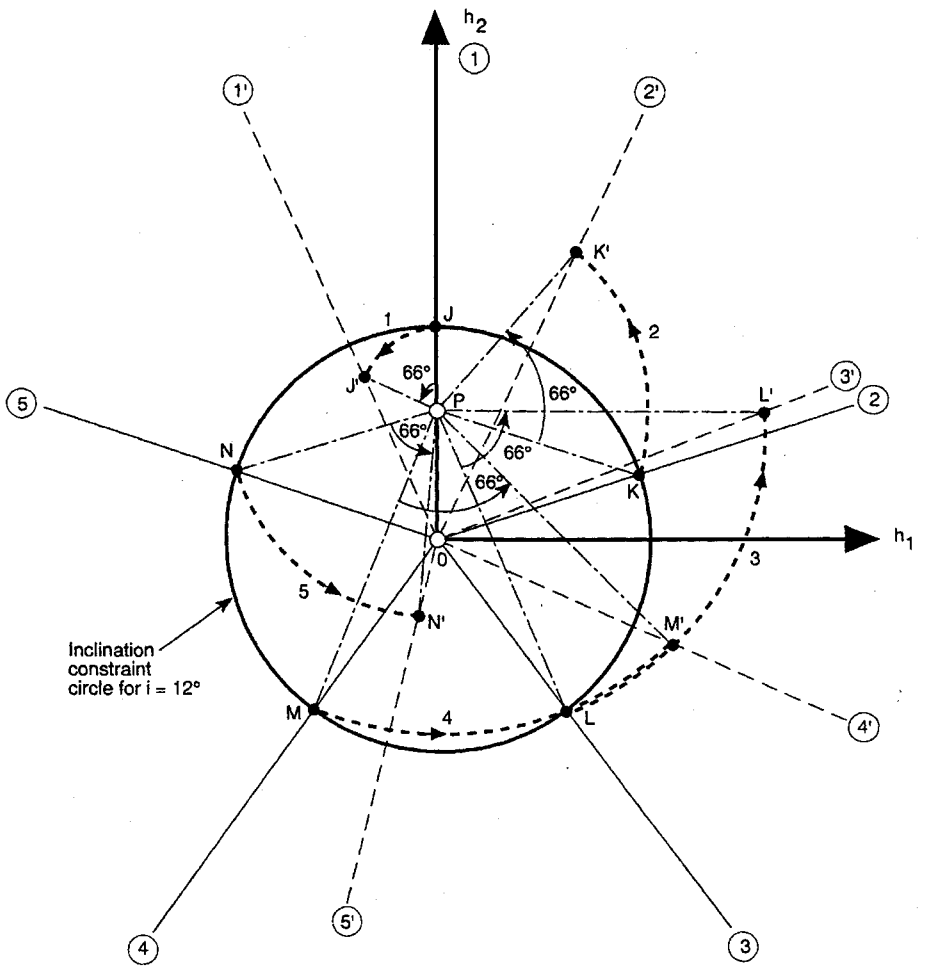

Fig. 3 Orbit plane precession of constellation with initial inclination of 12 deg and initial nodes of 0, 72, 144, 216, and 288 deg.

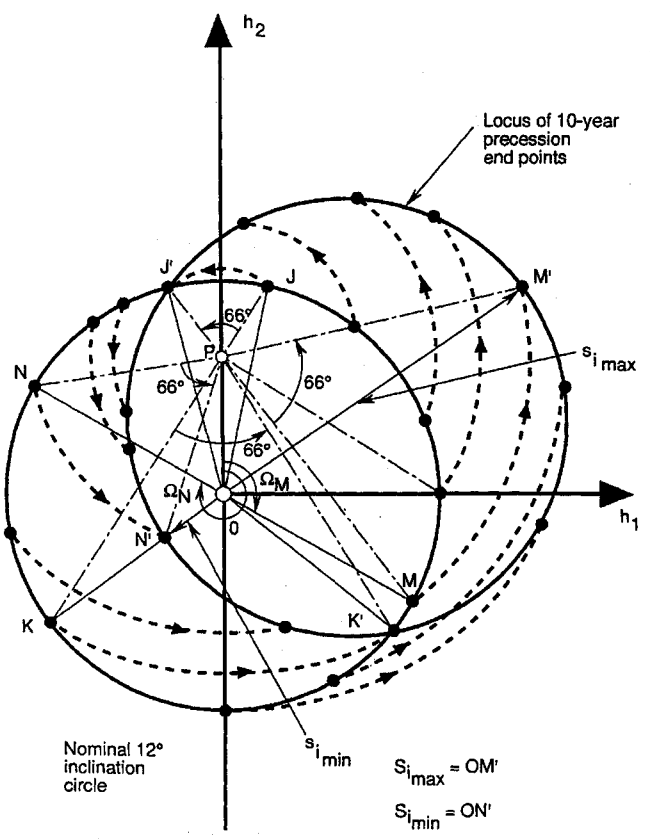

Fig. 4 Locus of 10-year precession endpoints for initial inclination of 12 deg.

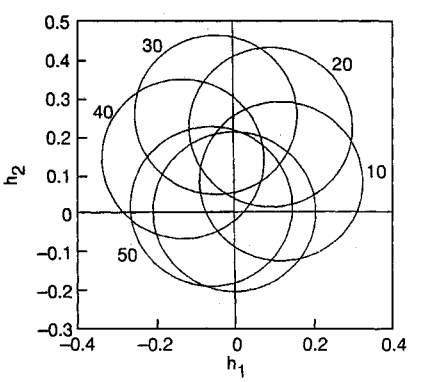

Fig. 5 Loci of 10-, 20-, 30-, 40-, and 50-year precession endpoints for initial inclination of 12 deg.

again evenly spaced in Ω. This scenario is then repeated until the 10-year satellite lifetime is consumed. The maximum ΔV needed by the most active satellite can, thus, be evaluated. Furthermore, the optimal initial configuration can also be determined to minimize this maximum ΔV budget. For larger inclination deadbands, such as in Fig. 2, it may be prohibitive to maneuver the vehicles back to the dotted target locus, requiring thereby the implementation of more elaborate targeting strategies to minimize fuel consumption over the mission lifetime.

Inclination Control Strategy with Analytic Orbit Prediction

Given an $i_{\min}$, $i_{\max}$ pair of inclination constraints, the coordinates of points E and G are first computed as follows. Point E is the intersection of the $s_{i_{\min}}$ constraint circle and the EF precession

circle of radius PF $= r_e = s_{i_{\max}} - h_{2e}$, where $h_{2e} = s_{7.5\,\deg}$, such that

$$h_1^2 + h_2^2 = s_{i_{\min}}^2 \tag{1}$$

$$h_1^2 + (h_2 - h_{2e})^2 = r_e^2 = \left(s_{i_{\max}} - h_{2e}\right)^2 \tag{2}$$

The solution is given by

$$(h_2)_E = s_{i_{\max}} - \frac{\left(s_{i_{\max}}^2 - s_{i_{\min}}^2\right)}{2h_{2e}} \tag{3}$$

$$(h_1)_E = \left[s_{i_{\min}}^2 - (h_2)_E^2\right]^{\frac{1}{2}} \tag{4}$$

The plus sign is chosen in front of the radical in Eq. (4) because point E will always be on the right-hand side of the diagram in Fig. 1, such that $(h_1)_E > 0$. The inclination and node are obtained from the general formulas

$$\Omega = \tan^{-1}(h_1/h_2) \tag{5}$$

$$i = \sin^{-1}\left[\left(h_1^2 + h_2^2\right)^{\frac{1}{2}}\right] \tag{6}$$

Point G is at the intersection of the circle of radius $s_{i_{\max}}$ and the precession circle GH of radius $r_g = \mathrm{PG} = s_{i_{\min}} + h_{2e}$, such that

$$h_1^2 + h_2^2 = s_{i_{\max}}^2 \tag{7}$$

$$h_1^2 + (h_2 - h_{2e})^2 = \left(s_{i_{\min}} + h_{2e}\right)^2 \tag{8}$$

The solution is given by

$$(h_2)_G = \frac{\left(s_{i_{\max}}^2 - s_{i_{\min}}^2\right)}{2h_{2e}} - s_{i_{\min}} \tag{9}$$

$$(h_1)_G = -\left[s_{i_{\max}}^2 - (h_2)_G^2\right]^{\frac{1}{2}} \tag{10}$$

Point G can be like point E either above or below the h_1 axis; however, $(h_1)_G < 0$ because G is always on the left-hand side of the h_1, h_2 diagram. Therefore, the minus sign must be adopted in front of the radical in Eq. (10). We now have evaluated the pairs (i_E, Ω_E) and (i_G, Ω_G) with, of course, $i_E = i_{\min}$ and $i_G = i_{\max}$. The regions I, II, III, and IV are defined, respectively, by the intervals $0 \le \Omega < \Omega_E$, $\Omega_E \le \Omega < \pi$, $\pi \le \Omega < \Omega_G$, and $\Omega_G \le \Omega < 2\pi$. At time zero, the orbits are evenly spaced in Ω and must be located on the target locus defined in Fig. 1. For region I, the initial orbit must be located on the circular arc FE at the intersection of this arc of equation $h_1^2 + (h_2 - h_{2e})^2 = (s_{i_{\max}} - h_{2e})^2$ and the line $h_1 = (\tan\Omega)h_2$. Solving for h_2 yields

$$h_2 = h_{2e}c_\Omega^2 \pm \left[h_{2e}^2 c_\Omega^4 + c_\Omega^2\left(s_{i_{\max}}^2 - 2h_{2e}s_{i_{\max}}\right)\right]^{\frac{1}{2}} \tag{11}$$

If $\Omega > \pi/2$, $h_2 < 0$ requires the selection of the minus sign in front of the radical. The term $(s_{i_{\max}} - 2h_{2e})$ can be either positive or negative depending on the value of $i_{\max}$. If $i_{\max} > 15.132$ deg, $(s_{i_{\max}} - 2h_{2e}) > 0$ such that the radical term in Eq. (11) is larger than the first term $h_{2e}c_\Omega^2$, this latter quantity being always positive. In this case, the two intersection points between the FE precession circle centered at P and the straight line $h_1 = (\tan\Omega)h_2$ are such that one is above the h_1 axis with $h_2 > 0$ and the other is below the h_1 axis with $h_2 < 0$, with the plus sign selected in front of the radical in the first case and the minus sign in the second case. If $i_{\max} < 15.132$ deg, then $(s_{i_{\max}} - 2h_{2e}) < 0$, and this time the intersection points are both above the h_1 axis with $h_2 > 0$. The radical term is now smaller than the leading $h_{2e}c_\Omega^2$ term with the plus sign corresponding to the higher intersection point. In either case, if $\Omega < \pi/2$,

$$h_2 = h_{2e}c_\Omega^2 + \left[h_{2e}^2 c_\Omega^4 + c_\Omega^2\left(s_{i_{\max}}^2 - 2h_{2e}s_{i_{\max}}\right)\right]^{\frac{1}{2}} \tag{12}$$

and if $\Omega > \pi/2$,

$$h_2 = h_{2e}c_\Omega^2 - \left[h_{2e}^2 c_\Omega^4 + c_\Omega^2\left(s_{i_{\max}}^2 - 2h_{2e}s_{i_{\max}}\right)\right]^{\frac{1}{2}} \tag{13}$$

Once h_2 is determined, the value of h_1 is obtained from $h_1 = (\tan\Omega)h_2$. For region II, we need $i = i_{\min}$ and, therefore, the coordinates of the corresponding initial orbit are given by

$$h_1 = s_{i_{\min}}s_\Omega \tag{14}$$

$$h_2 = s_{i_{\min}}c_\Omega \tag{15}$$

Similarly, for region IV, we need $i = i_{\max}$ and, therefore,

$$h_1 = s_{i_{\max}}s_\Omega \tag{16}$$

$$h_2 = s_{i_{\max}}c_\Omega \tag{17}$$

For region III, given an Ω, the h_1, h_2 coordinates at time zero are given by the intersection of the GH precession circle centered at P with equation $h_1^2 + (h_2 - h_{2e})^2 = (s_{i_{\min}} + h_{2e})^2$ and the straight line $h_1 = (\tan\Omega)h_2$. The solution is given by

$$h_2 = h_{2e}c_\Omega^2 \pm \left[h_{2e}^2 c_\Omega^4 + c_\Omega^2\left(s_{i_{\min}}^2 + 2h_{2e}s_{i_{\min}}\right)\right]^{\frac{1}{2}} \tag{18}$$

Even though $\Omega > \pi$, such that $h_1 < 0$, h_2 can be either positive or negative depending on whether $\Omega > 3\pi/2$. Because $(s_{i_{\min}}^2 + 2h_{2e}s_{i_{\min}})$ is always positive, the radical term in Eq. (18) is always larger than the positive first term $h_{2e}c_\Omega^2$ such that the two solutions corresponding to the two intersection points are always with $h_2 > 0$ for the first point and $h_2 < 0$ for the other point because these two points can never be on the same side of the h_1 axis with the same sign for their h_2 values. Therefore, if $\Omega < 3\pi/2$,

$$h_2 = h_{2e}c_\Omega^2 - \left[h_{2e}^2 c_\Omega^4 + c_\Omega^2\left(s_{i_{\min}}^2 + 2h_{2e}s_{i_{\min}}\right)\right]^{\frac{1}{2}} \tag{19}$$

and if $\Omega > 3\pi/2$,

$$h_2 = h_{2e}c_\Omega^2 + \left[h_{2e}^2 c_\Omega^4 + c_\Omega^2\left(s_{i_{\min}}^2 + 2h_{2e}s_{i_{\min}}\right)\right]^{\frac{1}{2}} \tag{20}$$

As before, the corresponding h_1 coordinate is obtained from $h_1 = (\tan\Omega)h_2$, and finally as for the case of region I, the intermediate value of the inclination $i_{\min} \le i \le i_{\max}$ is obtained from Eq. (21) without ambiguity:

$$i = \sin^{-1}\left[\left(h_1^2 + h_2^2\right)^{\frac{1}{2}}\right] \tag{21}$$

For a given initial set Ω_1, Ω_2, Ω_3, Ω_4, and Ω_5 separated by $360/5 = 72$ deg each, the initial h_1, h_2 coordinates of all five satellites are computed according to the regions where they are initially lying, and these coordinates are then predicted forward in time using the analytic circular precession approximation discussed earlier. Given a time Δt, e.g., of the order of a few days, and given the precession angular velocity $\omega = 2\pi/P$, where P is the period of these precessions centered at P with a value of roughly 54 years, the angular motion $\Delta\theta'' = \omega\Delta t$ is first calculated, after which the radius of the particular precession circle is evaluated from

$$r = \left\{h_1^2(i) + [h_2(i) - h_{2e}]^2\right\}^{\frac{1}{2}} \tag{22}$$

Next an angle ε is computed from[2]

$$\varepsilon = \tan^{-1}\left[\frac{h_1(i)}{h_{2e} - h_2(i)}\right] \tag{23}$$

the linear distance d from $d = 2r\sin(\Delta\theta''/2)$, and, finally, the predicted coordinates, from Ref. 18,

$$h_1(i+1) = h_1(i) + d\cos[\varepsilon + (\Delta\theta''/2)] \tag{24}$$

$$h_2(i+1) = h_2(i) + d\sin[\varepsilon + (\Delta\theta''/2)] \tag{25}$$

Table 1 Accumulated individual satellite ΔV in 4000 days with inclination control and specified initial nodes

	Satellite 1 ($\Omega_1 = 0$ deg)	Satellite 2 ($\Omega_2 = 72$ deg)	Satellite 3 ($\Omega_3 = 144$ deg)	Satellite 4 ($\Omega_4 = 216$ deg)	Satellite 5 ($\Omega_5 = 288$ deg)
ΔV, m/s	322.611	430.421	215.374	350.309	107.558

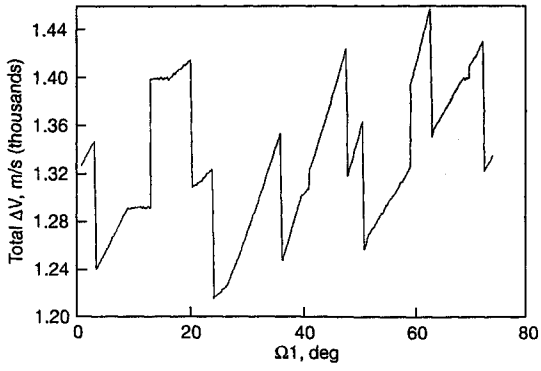

Fig. 6 Total ΔV requirements with inclination control for five-satellite constellation at nominal 12-deg inclination and ±1-deg tolerance vs initial node configuration for 4000-day lifetime.

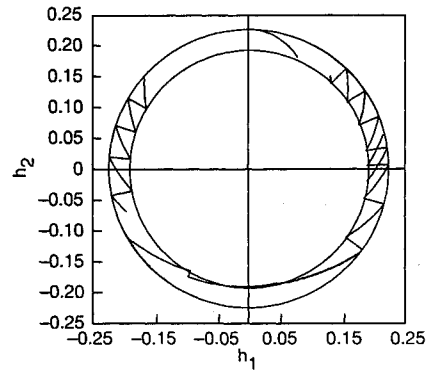

Fig. 7 Inclination-controlled constellation trajectories for optimal initial node configuration of $\Omega_1 = 24.3$, $\Omega_2 = 96.3$, $\Omega_3 = 168.3$, $\Omega_4 = 240.3$, and $\Omega_5 = 312.3$ deg over 4000-day lifetime.

with time $i + 1$ being equal to $i + \Delta t$. These calculations are repeated every Δt step for each of the satellites in the constellation, and their trajectories in the h_1, h_2 plane are described. At each step, the inclination of each satellite orbit is tested for possible violation of the $i_{\min}$ or $i_{\max}$ constraints. As soon as a violation occurs, that satellite orbit inclination is retargeted to the target locus curve, leaving its node unchanged. The ΔV needed for the inclination adjust maneuver is evaluated from $\Delta V = 2V \sin(i^*/2)$, where V is the geosynchronous orbit velocity $V = \sqrt{(\mu_e/a_s)}$ with $\mu_e = 398{,}601.3$ km^3/s^2, the Earth gravity constant, and $a_s = 42{,}164$ km, the orbit semimajor axis, and where i^* is the wedge angle between the premaneuver and postmaneuver orbits given by the Ω_1, i_1 and Ω_1, i_2 pairs, respectively[18]:

$$c_{i^*} = s_{i_1} s_{i_2} + c_{i_1} c_{i_2} \tag{26}$$

where i_2 is, of course, the target inclination that will place that particular orbit on the target locus for another period of maneuver-free precession. Each satellite maneuvers a number of times during a predefined constellation lifetime, e.g., 10 years, and the total ΔV needed by each satellite is evaluated by adding the individual small ΔV as they occur. If we now add the total ΔV from each satellite, then the overall ΔV_{tot} needed by all five satellites can be calculated. This calculation is repeated for each value of the initial Ω_1, and, therefore, $\Omega_2, \ldots, \Omega_5$ values because they are incremented by 72 deg at time zero, and the total ΔV_{tot} is plotted vs Ω_1, as in Fig. 6 with Ω_1 varying between 0 and 72 deg. The minimum ΔV_{tot} occurs for $\Omega_1 = 24.3$ deg at 1216 m/s over a period of 4000 days, whereas the maximum ΔV_{tot} corresponds to an initial $\Omega_1 = 63$ deg at 1456 m/s.

Figure 7 shows the trajectories of the five satellites for the overall ΔV minimizing initial configuration given by $\Omega_1 = 24.3$, $\Omega_2 = 96.3$, $\Omega_3 = 168.3$, $\Omega_4 = 240.3$, and $\Omega_5 = 312.3$ deg nodal values. Figure 8 shows the variation of the nodes over the same 4000-day lifetime for an initial configuration given by $\Omega_1 = 0$, $\Omega_2 = 72$, $\Omega_3 = 144$, $\Omega_4 = 216$, and $\Omega_5 = 288$ deg. Because the nodes are left uncontrolled, the even nodal spacing is quickly distorted, as was clear from the preceding graphical general discussion. The h_1, h_2 trajectories in the latter example show that spacecraft 1, 2, 3, 4, and 5 require, respectively, 1, 3, 4, 1, and 4 inclination adjust maneuvers. The accumulated ΔV for each satellite is shown in Table 1.

Inclination Control and Node Adjust Maneuver Strategy with Analytic Orbit Prediction

The nodal distortion is now controlled using a simple strategy that consists of adjusting the nodal spacing at each inclination control

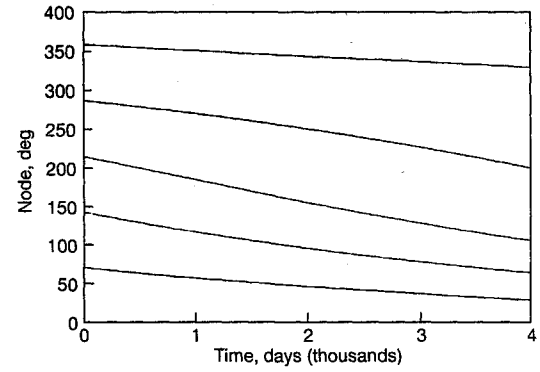

Fig. 8 Uncontrolled nodal variation of constellation over 4000-day lifetime for initial $\Omega_1 = 0$, $\Omega_2 = 72$, $\Omega_3 = 144$, $\Omega_4 = 216$, and $\Omega_5 = 288$ deg.

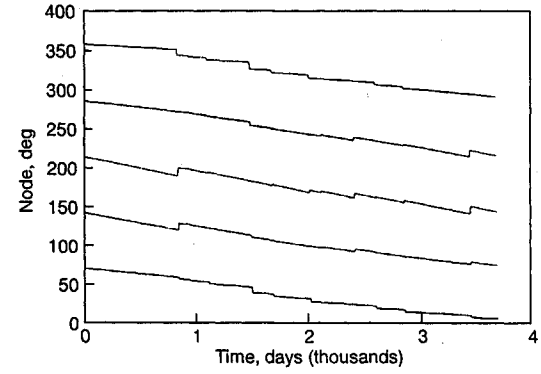

Fig. 9 Controlled nodal variation of constellation over 3650-day lifetime for initial $\Omega_1 = 0$, $\Omega_2 = 72$, $\Omega_3 = 144$, $\Omega_4 = 216$, and $\Omega_5 = 288$ deg.

event. The vehicle carrying out an inclination change maneuver leaves its node unchanged as before. However, the other four vehicles, which do not require any inclination change at this stage, adjust their respective nodes such that, with respect to the vehicle that is performing an inclination change, the even nodal spacing is recovered, meaning that all five nodes are equally distributed once again with a spacing of 72 deg. Figure 9 shows the evolution of the constellation satellite nodes over a 3650-day period for an initial configuration given by $\Omega_1 = 0$, $\Omega_2 = 72$, $\Omega_3 = 144$, $\Omega_4 = 216$, and $\Omega_5 = 288$ deg, with no excessive distortion.

Table 2 Accumulated individual satellite ΔV in 3650 days with inclination and node control and specified initial nodes

	Satellite 1	Satellite 2	Satellite 3	Satellite 4	Satellite 5
Initial node	$\Omega_1 = 0$ deg	$\Omega_2 = 72$ deg	$\Omega_3 = 144$ deg	$\Omega_4 = 216$ deg	$\Omega_5 = 288$ deg
ΔV, m/s	528.867	552.639	436.577	559.457	564.554
Initial node	$\Omega_1 = 33.1$	$\Omega_2 = 105.1$	$\Omega_3 = 177.1$	$\Omega_4 = 249.1$	$\Omega_5 = 321.1$
ΔV	435.897	489.508	506.379	369.913	563.011

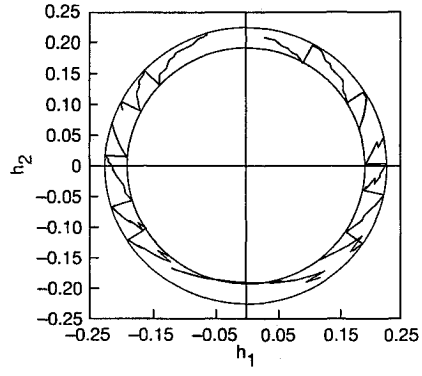

Fig. 10 Constellation trajectories over 3650-day lifetime with both inclination and node control for initial $\Omega_1 = 0$, $\Omega_2 = 72$, $\Omega_3 = 144$, $\Omega_4 = 216$, and $\Omega_5 = 288$ deg.

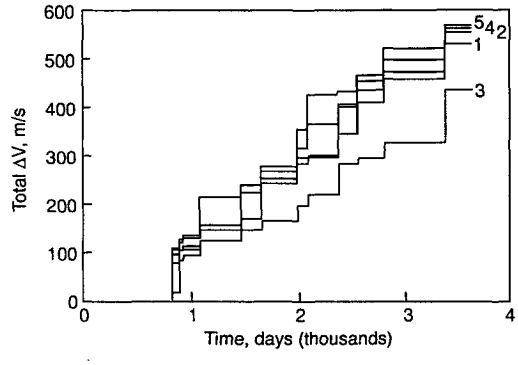

Fig. 11 Individual accumulated total ΔV requirements over 3650-day lifetime with inclination and node control for initial $\Omega_1 = 0$, $\Omega_2 = 72$, $\Omega_3 = 144$, $\Omega_4 = 216$, and $\Omega_5 = 288$ deg.

Figure 10 shows the five satellites' polar trajectories with the nodal maneuvers represented by the short circumferential instantaneous adjustments at constant i while the inclination change maneuvers are performed by instantaneous radial adjustments at constant Ω. The remaining portions of these trajectories are made of circular arcs representing the precessions of the five orbit planes by analytic approximation. The accumulated ΔV for each spacecraft is shown in Fig. 11, where all satellites are maneuvering simultaneously with total ΔV at the 3650-day mark for satellites 1–5 shown in Table 2. The inclination time histories show small discontinuities in the inclination rates, which are due to the changing node carried out impulsively at the times of inclination adjust maneuvers performed by the other vehicles. The combined total ΔV for all five satellites stands at 2642.096 m/s. If we now compute this total ΔV for values of Ω_1 spanning the interval (0, 72) deg, we can produce the plot in Fig. 12, which shows that the optimal initial configuration that results in the lowest total ΔV over the 3650-day lifetime of the constellation is given by $\Omega_1 = 33.1$, $\Omega_2 = 105.1$, $\Omega_3 = 177.1$, $\Omega_4 = 249.1$, and $\Omega_5 = 321.1$ deg with a corresponding ΔV_{tot} of 2364.709 m/s and individual satellite totals shown in Table 2.

The two strategies discussed so far made use of the analytic approximation in describing the orbit plane precessions. The next section revisits the strategy of the preceding section by replacing the circular precessions, which are epoch independent, by more exacting representations of those precessions, which are now simulated by numerically integrating the differential equations for i and Ω,

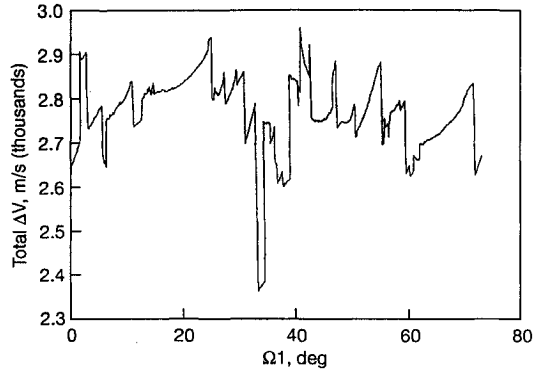

Fig. 12 Total ΔV requirements for five-satellite constellation over 3650-day lifetime with inclination and node control vs initial node configuration.

properly accounting, thereby, for the epoch dependency of the orbit plane motion.

Inclination Control Strategy with Numerical Orbit Propagation

The orbit plane orientation parameters obey the following differential equations in circular orbit:

$$\dot{i} = -\frac{1}{na^2 s_i}\frac{\partial R}{\partial \Omega} \tag{27}$$

$$\dot{\Omega} = \frac{1}{na^2 s_i}\frac{\partial R}{\partial i} \tag{28}$$

where R is the perturbing function due to J_2 and the lunisolar gravity given by Ref. 9:

$$R = \tfrac{1}{4}\mu n_m^2 a^2\left[\left(1-\tfrac{3}{2}s_i^2\right)\left(1-\tfrac{3}{2}s_{i_m}^2\right) + \tfrac{3}{4}s_{2i}s_{2i_m}c_{\Omega-\Omega_m} + \tfrac{3}{4}s_i^2 s_{i_m}^2 c_{2(\Omega-\Omega_m)}\right] + \tfrac{1}{4}n_s^2 a^2\left[\left(1-\tfrac{3}{2}s_i^2\right)\left(1-\tfrac{3}{2}s_{i_s}^2\right) + \tfrac{3}{4}s_{2i}s_{2i_s}c_\Omega + \tfrac{3}{4}s_i^2 s_{i_s}^2 c_{2\Omega}\right] + \tfrac{3}{4}n^2 J_2 R_e^2\left(\tfrac{1}{3}-\tfrac{1}{2}s_i^2\right) \tag{29}$$

with n and a the satellite orbit mean motion and semimajor axis. The lunar i_m and Ω_m vary according to

$$c_{i_m} = c_{i_M}c_{i_s} - s_{i_s}s_{i_M}c_{\Omega_M} \tag{30}$$

$$s_{\Omega_m} = \frac{s_{i_M}s_{\Omega_M}}{s_{i_m}} \tag{31}$$

where $i_M = 5.145$ deg is the ecliptic inclination of the moon's orbit and $\Omega_M = 259.183 - 0.05295t$, in degrees, is its ascending node, which regresses linearly in time due to the solar gravity. Here t is measured in Julian days from the epoch of Jan. 1, 1900, at 12 h (Ref. 9). The regression period of Ω_M is roughly equal to 18.6 years, such that the Ω_M equation shown after Eq. (31) is also adopted with the epoch of Jan. 1, 1993, at 12 h, adding roughly five regression cycles to the original epoch. This rough calculation is done only for illustration purposes to show the effect of epoch selection on the optimal $\Omega_1, \ldots, \Omega_5$ at simulation start and thereby the total ΔV requirements. The *Astronomical Almanac* lists Ω_M exactly as $\Omega_M = 279.854 - 0.05295d$, in degrees, where d is the interval in days from

Jan. 1, 1992, at 0 h. Now the adoption of the nonsingular variables $h_1 = s_i s_\Omega$ and $h_2 = s_i c_\Omega$ (in Ref. 9) led to the nonsingular set

$$\dot{h}_1 = \frac{c_i}{na^2}\frac{\partial R}{\partial h_2} \tag{32}$$

$$\dot{h}_2 = \frac{-c_i}{na^2}\frac{\partial R}{\partial h_1} \tag{33}$$

For $i < \pi/2$, we have $c_i = (1-h_1^2-h_2^2)^{1/2}$ because for all $0 \le i \le \pi$, $s_i = (h_1^2+h_2^2)^{1/2}$, $c_{2i} = (1-2h_1^2-2h_2^2)$. Restricting ourselves to $c_i > 0$ or $i < \pi/2$, we also have $s_i c_i = (h_1^2+h_2^2)^{1/2}(1-h_1^2-h_2^2)^{1/2}$. From $s_\Omega = h_1/s_i$ and $c_\Omega = h_2/s_i$, we also have $s_{2\Omega} = 2h_1h_2/s_i^2$ and $c_{2\Omega} = (h_2^2-h_1^2)/s_i^2$, as well as

$$c_{\Omega-\Omega_m} = (h_2/s_i)c_{\Omega_m} + (h_1/s_i)s_{\Omega_m} \tag{34}$$

$$s_{\Omega-\Omega_m} = (h_1/s_i)c_{\Omega_m} - (h_2/s_i)s_{\Omega_m} \tag{35}$$

$$c_{2(\Omega-\Omega_m)} = \frac{\left(h_2^2-h_1^2\right)}{s_i^2}c_{2\Omega_m} + \frac{2h_1h_2}{s_i^2}s_{2\Omega_m} \tag{36}$$

$$s_{2(\Omega-\Omega_m)} = \frac{2h_1h_2}{s_i^2}c_{2\Omega_m} - \frac{\left(h_2^2-h_1^2\right)}{s_i^2}s_{2\Omega_m} \tag{37}$$

Equations (32) and (33) can be written directly in terms of h_1 and h_2 by making the following manipulations:

$$\frac{\partial R}{\partial h_1} = \frac{\partial R}{\partial i}\frac{\partial i}{\partial h_1} + \frac{\partial R}{\partial \Omega}\frac{\partial \Omega}{\partial h_1} = \frac{\partial R}{\partial i}\frac{h_1}{s_i c_i} + \frac{\partial R}{\partial \Omega}\frac{h_2}{s_i^2}$$

and

$$\frac{\partial R}{\partial h_2} = \frac{\partial R}{\partial i}\frac{\partial i}{\partial h_2} + \frac{\partial R}{\partial \Omega}\frac{\partial \Omega}{\partial h_2} = \frac{\partial R}{\partial i}\frac{h_2}{s_i c_i} - \frac{\partial R}{\partial \Omega}\frac{h_1}{s_i^2}$$

We have

$$\frac{\partial R}{\partial i} = \frac{1}{4}\mu n_m^2 a^2\left[-3s_i c_i\left(1-\frac{3}{2}s_{i_m}^2\right) + \frac{3}{2}c_{2i}s_{2i_m}c_{\Omega-\Omega_m} + \frac{3}{2}s_i c_i s_{i_m}^2 c_{2(\Omega-\Omega_m)}\right] + \frac{1}{4}n_s^2 a^2\left[-3s_i c_i\left(1-\frac{3}{2}s_{i_s}^2\right) + \frac{3}{2}c_{2i}s_{2i_s}c_\Omega + \frac{3}{2}s_i c_i s_{i_s}^2 c_{2\Omega}\right] - \frac{3}{2}n^2 J_2 R_e^2 s_i c_i \tag{38}$$

$$\frac{\partial R}{\partial \Omega} = \frac{1}{4}\mu n_m^2 a^2\left[-\frac{3}{4}s_{2i}s_{2i_m}s_{\Omega-\Omega_m} - \frac{3}{2}s_i^2 s_{i_m}^2 s_{2(\Omega-\Omega_m)}\right] + \frac{1}{4}n_s^2 a^2\left(-\frac{3}{4}s_{2i}s_{2i_s}s_\Omega - \frac{3}{2}s_i^2 s_{i_s}^2 s_{2\Omega}\right) \tag{39}$$

After making the proper substitutions, the final form of the differential equations of motion is obtained:

$$\frac{dh_1}{dt} = \frac{\mu}{4n}n_m^2\left\{-3h_2\left(1-\frac{3}{2}s_{i_m}^2\right)\left(1-h_1^2-h_2^2\right)^{\frac{1}{2}} + \frac{3}{2}s_{2i_m}\left[c_{\Omega_m}\left(1-h_1^2-h_2^2\right) - h_2\left(h_2c_{\Omega_m}+h_1s_{\Omega_m}\right)\right] + \frac{3}{2}s_{i_m}^2\left(1-h_1^2-h_2^2\right)^{\frac{1}{2}}\left(h_2c_{2\Omega_m}+h_1s_{2\Omega_m}\right)\right\} + \frac{n_s^2}{4n}\left[-3h_2\left(1-\frac{3}{2}s_{i_s}^2\right)\left(1-h_1^2-h_2^2\right)^{\frac{1}{2}} + \frac{3}{2}s_{2i_s}\left(1-h_1^2-2h_2^2\right) + \frac{3}{2}s_{i_s}^2h_2\left(1-h_1^2-h_2^2\right)^{\frac{1}{2}}\right] - \frac{3}{2a^2}nJ_2R_e^2h_2\left(1-h_1^2-h_2^2\right)^{\frac{1}{2}} \tag{40}$$

$$\frac{dh_2}{dt} = -\frac{\mu}{4n}n_m^2\left\{-3h_1\left(1-\frac{3}{2}s_{i_m}^2\right)\left(1-h_1^2-h_2^2\right)^{\frac{1}{2}} + \frac{3}{2}s_{2i_m}\left[s_{\Omega_m}\left(1-h_1^2-h_2^2\right) - h_1\left(h_2c_{\Omega_m}+h_1s_{\Omega_m}\right)\right] + \frac{3}{2}s_{i_m}^2\left(1-h_1^2-h_2^2\right)^{\frac{1}{2}}\left(h_2s_{2\Omega_m}-h_1c_{2\Omega_m}\right)\right\} - \frac{n_s^2}{4n}\left[-3h_1\left(1-\frac{3}{2}s_{i_s}^2\right)\left(1-h_1^2-h_2^2\right)^{\frac{1}{2}} - \frac{3}{2}s_{2i_s}h_1h_2 - \frac{3}{2}s_{i_s}^2h_1\left(1-h_1^2-h_2^2\right)^{\frac{1}{2}}\right] + \frac{3}{2}\frac{n}{a^2}h_1J_2R_e^2\left(1-h_1^2-h_2^2\right)^{\frac{1}{2}} \tag{41}$$

with $i_s = 23.445$ deg, $J_2 = 1.0827 \times 10^{-3}$, and $R_e = 6378.14$ km.

We can now revisit the strategy of the section "Inclination Control Strategy with Analytic Orbit Prediction" and replace the circular precession arcs by the more exacting precessions obtained by numerically integrating Eqs. (40) and (41). The maneuvers are triggered as before as soon as one of the two inclination constraint circles is violated. The values of Ω_M and, therefore, of i_m and Ω_m are varied during the integration according to the expressions just shown. Figures 13 and 14 show how these trajectories are affected by the initial epoch, meaning the lunar orbit ecliptic node and, therefore, the subsequent i_m, Ω_m variations affecting the perturbations due to the moon. These figures are generated, respectively, with $\Omega_M = 259.183 - 0.05295t$ and $\Omega_M = 329.283 - 0.05295t$ corresponding to an epoch of +15 years from the original epoch that is valid for the first Ω_M expression. The subsequent Ω_M value is obtained by subtracting an angle of 96.633 deg for every

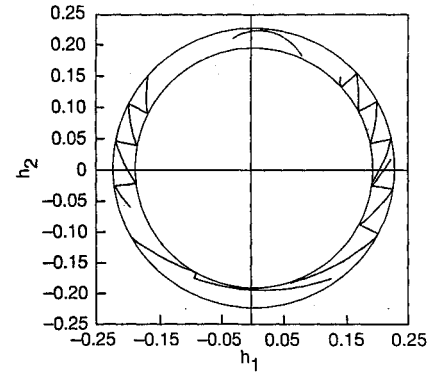

Fig. 13 Numerically integrated constellation trajectories over 3650-day lifetime with inclination control for initial Ω_1 = 24.3, Ω_2 = 96.3, Ω_3 = 168.3, Ω_4 = 240.3, and Ω_5 = 312.3 deg and lunar orbit $\Omega_M = 259.183 - 0.05295t$ deg.

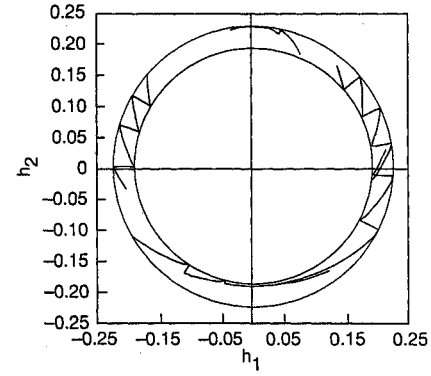

Fig. 14 Numerically integrated constellation trajectories over 3650-day lifetime with inclination control for initial Ω_1 = 24.3, Ω_2 = 96.3, Ω_3 = 168.3, Ω_4 = 240.3, and Ω_5 = 312.3 deg and lunar orbit $\Omega_M = 329.283 - 0.05295t$ deg.

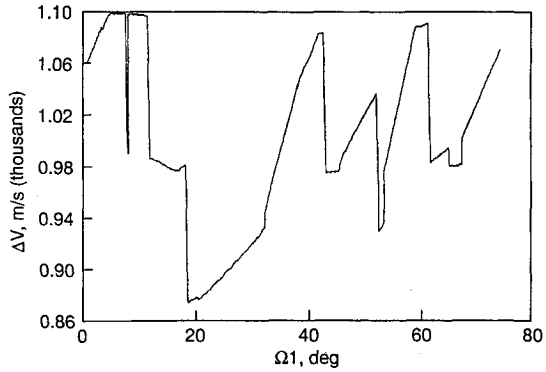

Fig. 15 Total ΔV requirements for five-satellite constellation with inclination control over 3650-day lifetime vs initial node configuration and lunar orbit $\Omega_M = 259.183 - 0.05295t$ deg at initial epoch.

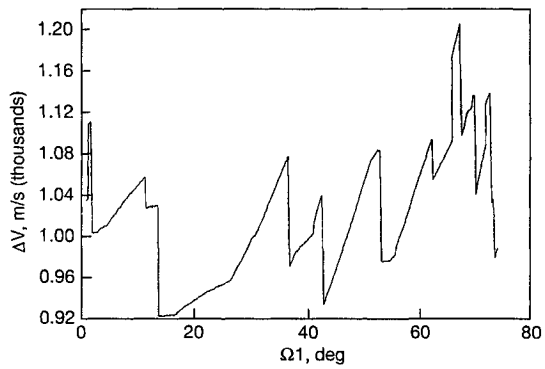

Fig. 16 Total ΔV requirements for five-satellite constellation with inclination control over 3650-day lifetime vs initial node configuration and lunar orbit $\Omega_M = 329.283 - 0.05295t$ deg at initial epoch.

5-year lunar orbit ecliptic nodal regression. These two epoch-dependent exact trajectories are for the initial configuration given by $\Omega_1 = 24.3$, $\Omega_2 = 96.3$, $\Omega_3 = 168.3$, $\Omega_4 = 240.3$, and $\Omega_5 = 312.3$ deg of Fig. 7, which was obtained analytically and which corresponded to the overall analytic minimum $-\Delta V$ solution shown in Fig. 6 for the slightly shorter 3650-day lifetime. Note how the trajectory of spacecraft 1 is affected by the Ω_M epoch, requiring several maneuvers as it repeatedly hits the outer inclination constraint.

The final two figures, namely, Figs. 15 and 16, show the cumulative total five-satellite ΔV requirements for the two epochs used earlier, as a function of initial even nodal configuration. There exists an appreciable variability in the ΔV requirements, as well as the initial constellation geometry, that leads to the minimum overall ΔV. Each of these last plots requires close to a 9-h run on a 486/66-MHz desktop computer using a 0.1-deg step to cover the range $0 \leq \Omega_1 \leq 72$ deg as opposed to only a few minutes for the analytic method used in the preceding sections. If a series of the exact plots is generated at 1-year epoch intervals spanning the entire 18.6-year regression cycle, then the optimum initial configuration as well as the optimum epoch within this cycle can be selected to provide the overall minimum-ΔV requirements. The same exacting simulations can also be carried out for the strategy of the preceding section, which adjusts the nodes periodically to establish the relevant minimum-ΔV requirements.

Concluding Remarks

Analytic and numerical simulations using a pair of simple suboptimal orbit maintenance strategies have been described to find the optimal initial orbit plane configuration of a constellation of five satellites in inclined geosynchronous orbits that results in minimum ΔV accumulated by the five satellites over the constellation lifetime. These orbit plane control strategies achieve either intermittent inclination adjust maneuvers that confine each satellite orbit within a user-defined inclination tolerance deadband centered at the common nominal inclination at all times or both inclination and node adjust maneuvers that, in addition, keep the initially evenly spaced nodal configuration from being distorted. In either case, the optimal initial nodal values as well as the inclinations are determined to minimize the total overall accumulated ΔV by all five satellites. The orientation of the orbit plane of the moon within its 18.6-year regression cycle is also shown to have an important effect on the total ΔV requirements of the constellation over its fixed lifetime, resulting in an optimal launch time for the constellation. The suboptimal orbit plane maintenance strategies developed are of a general nature, meaning that they are not restricted to a given number of satellites, their common nominal inclination, or a prespecified lifetime. These solutions approach the true minimum-ΔV from above; the minimum-ΔV solution itself requires consideration of the complete state-constrained cooperative differential game, which is quite difficult to analyze. Further savings in fuel are possible by using electric engines and designing the appropriate maneuvering strategies to replace the impulsive strategies adopted here.

Acknowledgment

This work was supported by the U.S. Air Force Space and Missile Systems Center under Contract F04701-88-C-0089.

References

[1]Musen, P., "On the Long-Period Luni-Solar Effect in the Motion of the Artificial Satellite," *Journal of Geophysical Research*, Vol. 66, No. 6, 1961, pp. 1659–1665.

[2]Musen, P., Bailie, A., and Upton, E., "Development of the Lunar and Solar Perturbations in the Motion of an Artificial Satellite," NASA TN D-494, Jan. 1961.

[3]Musen, P., "On the Long-Period Lunar and Solar Effects on the Motion of an Artificial Satellite, 2," *Journal of Geophysical Research*, Vol. 66, No. 9, 1961, pp. 2797–2805.

[4]Frick, R. H., and Garber, T. B., "Perturbations of a Synchronous Satellite," Rand Corp., Rept. R-399-NASA, Santa Monica, CA, May 1962.

[5]Allen, R. R., and Cook, G. E., "The Long-Period Motion of the Plane of a Distant Circular Orbit," *Proceedings of the Royal Society*, Vol. 280, No. 1380, 1964, pp. 97–109.

[6]Billik, B. H., "Cross-Track Sustaining Requirements for a 24-hr Satellite," *Journal of Spacecraft and Rockets*, Vol. 4, No. 3, 1967, pp. 297–301.

[7]Frick, R. H., "Orbital Regression of Synchronous Satellites Due to the Combined Gravitational Effects of the Sun, the Moon, and the Oblate Earth," Rand Corp., Rept. R-454-NASA, Santa Monica, CA, Aug. 1967.

[8]Balsam, R. E., "A Simplified Approach for Correction of Perturbations on a Stationary Orbit," *Journal of Spacecraft and Rockets*, Vol. 6, No. 7, 1969, pp. 805–811.

[9]Kamel, A., and Tibbitts, R., "Some Useful Results on Initial Node Locations for Near-Equatorial Circular Satellite Orbits," *Celestial Mechanics*, Vol. 8, 1973, pp. 45–73.

[10]Kamel, A. A., "Synchronous Satellite Ephemeris Due to Earth's Triaxiality and Luni-Solar Effects," AIAA Paper 78-1441, Aug. 1978.

[11]Eckstein, M. C., and Hechler, F., "Optimal Autonomous Stationkeeping of Geostationary Satellites," American Astronautical Society, AAS Paper 81-206, Aug. 1981.

[12]Kamel, A. A., and Wagner, C. A., "On the Orbital Eccentricity Control of Synchronous Satellites," *Journal of the Astronautical Sciences*, Vol. 30, No. 1, 1982, pp. 61–73.

[13]Kamel, A. A., "Geosynchronous Satellite Perturbations Due to Earth's Triaxiality and Luni-Solar Effects," *Journal of Guidance, Control, and Dynamics*, Vol. 5, No. 2, 1982, pp. 189–193.

[14]Slavinskas, D. D., Johnson, G. K., and Benden, W. J., "Efficient Inclination Control for Geostationary Satellite," AIAA Paper 85-0216, Jan. 1985.

[15]Murdoch, J., and Pocha, J. J., "The Orbit Dynamics of Satellite Clusters," 33rd International Astronautical Congress, International Astronautical Federation, IAF Paper 82-54, Paris, France, Sept.–Oct. 1982.

[16]Walker, J. G., "The Geometry of Satellite Clusters," Royal Aircraft Establishment, Rept. RAE-TR-81084, Farnborough, England, UK, July 1981.

[17]Hubert, S., and Swale, J., "Stationkeeping of a Constellation of Geostationary Communication Satellites," AIAA Paper 84-2024, Aug. 1984.

[18]Kechichian, J. A., "Optimal Steering for North–South Stationkeeping of Geostationary Spacecraft," *Journal of Guidance, Control, and Dynamics*, Vol. 20, No. 3, 1997, pp. 435–444; also American Astronautical Society, AAS Paper 95-118, Feb. 1995.

J. D. Gamble
Associate Editor